Determining the shape of reflectance reference samples for curved surface reflectors

OPEN ACCESS
IOP Publishing
Measurement Science and Technology
Meas. Sci. Technol. **31** (2020) 054010 (8pp)
https://doi.org/10.1088/1361-6501/ab68bf

Determining the shape of reflectance reference samples for curved surface reflectors

Dmitri Lanevski[1], Farshid Manoocheri[1], Anna Vaskuri[1], Jacques Hameury[3], Robert Kersting[4], Christian Monte[5], Albert Adibekyan[5], Elena Kononogova[5] and Erkki Ikonen[1,2]

[1] Metrology Research Institute, Aalto University, Espoo, Finland
[2] VTT MIKES, Espoo, Finland
[3] Laboratoire National de Métrologie et d'Essais (LNE), Trappes, France
[4] Fraunhofer-Institute for Production Systems and Design Technology (IPK), Berlin, Germany
[5] Physikalisch-Technische Bundesanstalt (PTB), Berlin, Germany

E-mail: dmitri.lanevski@aalto.fi

Received 29 July 2019, revised 15 December 2019
Accepted for publication 7 January 2020
Published 5 March 2020

Abstract

Foils made of different materials are often used as reflective insulators. Many manufacturers aim to accurately measure their optical properties to estimate and improve their performance. However, flat reflectance reference samples used in measurements do not correctly represent reflective insulators and cause discrepancies between different measurement techniques. The current work presents a method for modelling surface shape of appropriate reflectance reference samples that could be produced by additive manufacturing. The method is based on studying the reflection distribution of reflective insulators and is described with an example of aluminium foil. The method's performance is validated using Monte-Carlo simulations.

Keywords reflectance, Monte-Carlo, reflective insulators, foil, curved surface, reference sample, additive manufacturing

(Some figures may appear in colour only in the online journal)

1. Introduction

Precise characterization of the reflectivity of reflective insulation products for buildings is important for manufacturers of those products. However, recent cross-comparison of reflectivity measurement techniques organized by the standardization working group CEN/TC 89/WG 12 has shown large differences of total hemispherical reflectivity results deviating by 6 % (from 0.92 to 0.98) on the same reflective material [1]. The comparison included 'integrating sphere' instruments and commercially available portable instruments (reflectometers) like TIR 100-2 from INGLAS. The reasons of these differences are yet to be explained, but one of them ought to be a reflectance reference sample that does not represent the measurement object closely enough.

As indicated in the cross-comparison, the plane mirrors or diffusing reflectance samples that are usually used for calibration of portable instruments may not be the best calibration targets. They are quite far from actual measurement targets—aluminized or aluminum foils that are usually used as external surfaces of reflective insulators. Foils are surface reflectors that are not strictly specular or diffuse reflectors since, to some extent, they exhibit both types of reflection. On top of that, they usually have non-flat (battered and crumpled) surfaces and their comparison with flat reference standards may introduce some additional variation in reflectivity measurements. Recent study showed that calibration factros obtained for NGLAS Produktions GmbH: TIR 100-2 using flat reference standards might not be applicable for mesh-reinforced foils [2].

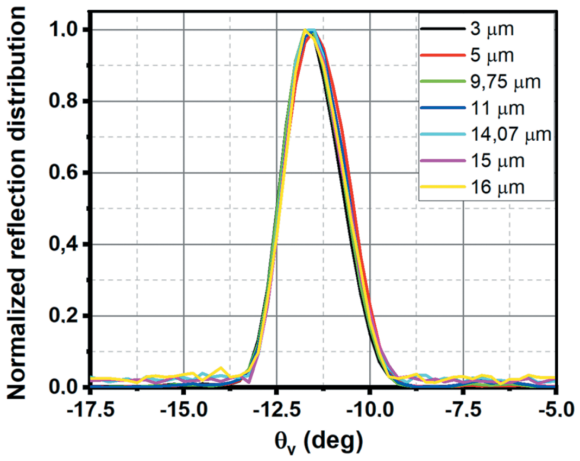

Figure 1. Reflection distribution functions of flattened foil bonded to a rigid support measured for different wavelengths.

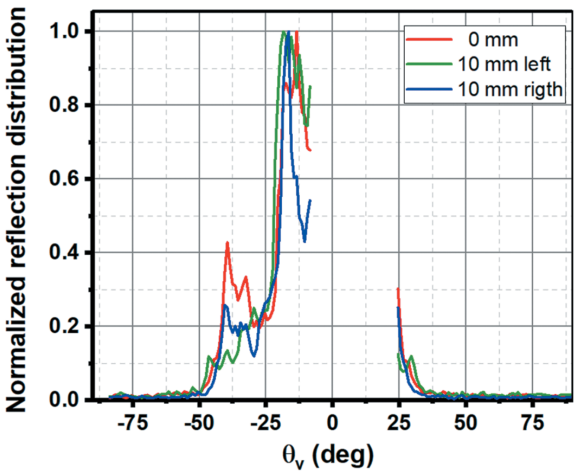

Figure 2. Reflection distribution functions of mesh-reinforced foil measured for different illumination spot positions.

Production of appropriate reference samples seems to be an obvious solution for this problem. Modern additive manufacturing methods allow to produce objects from almost any material with almost any size and shape. The questions that remain are that what should be the sample's surface shape so that it would exhibit reflectance properties similar to the reflective insulation products and what would be a suitable manufacturing method.

Present article tackles these problems by introducing a method to determine a shape of the new reflectance reference sample that could be manufactured by precise additive manufacturing or by some other method.

2. Angular distribution of reflection of aluminum foil

Characterization of one of the most common reflective insulator—aluminium foil—was a starting point in our research. For this reason, several measurements of angular reflection distribution of different aluminium foil samples were performed. They were conducted at the Laboratoire national de métrologie et d'essais (LNE) using an absolute reflectometer developed for reflectance calibration of mirrors in the infrared [3].

First, a flat aluminium foil bonded to a solid rigid support was measured. It was illuminated by IR light with wavelengths varying from 3 to 16 μm corresponding to common insulatiove materials exploitation temperatures ranging from 20 °C to 25 °C. To get better signal-to-noise ratio an IR light from the black body of 1850 K and interference filters were used to filter wavelengths of interest. Illumination had spot size of 12 mm and $\theta_i = 11.5°$ angle of incidence (from the sample normal). Reflected light was measured in the same plane ($\varphi = 0°$) from $\theta_v = -5°$ to $-18°$ with respect to sample's normal or approximately $\pm 6°$ around specular reflection direction. The results can be seen in figure 1.

Flattened aluminium foil's angular distribution of reflection was mostly specular and exhibited only $\pm 2.5°$ beam dispersion around specular direction. Nevertheless, it indicated that the foil surface is not completely smooth and has some microstructure that should be taken into account during development of new reference samples. Illumination wavelength variation had a little effect on the reflection angular distribution.

In the same conditions, another sample—mesh-reinforced aluminium foil—was attempted to be measured. However, used sample strongly scattered filtered individual wavelengths and signal-to-noise ratio was not sufficient for reliable results. For this reason, unfiltered 1850K black body illumination was used for illumination. Beam size remained the same, but angle of incidence changed to 8°. Illumination spot position was also varied to investigate changes of angular reflection distribution caused by non-uniformity of the sample. Results are depicted in figure 2.

Mesh-reinforced aluminium foil exhibited $\pm 40°$ beam dispersion and confirmed that macroscopic surface structures have a large effect on resulting angular distribution of reflection. Variation of the illumination spot position did not have a big effect on beam dispersion extent. However, it affected the shape of angular distribution and indicated a non-uniformity of the sample surface.

Ultimately, the conducted measurements showed that to produce a reflectance reference sample with reflection properties of an actual insulator material, one should determine its microstructure as well as macrostructure. Furthermore, the macrostructure might be more important since its effect on the angular distribution of reflection is greater.

3. Determining the shape of reflectance reference sample

There are many possibilities to determine the topology of the reference sample under development. Simplest methods imply 3D scanning of the surface of the actual reference sample and producing copy of it using additive manufacturing. However, mesh reinforced foil structure may be highly irregular and reflectivity distribution may change significantly when sample with similar structure is realigned under illumination beam. Therefore, to design a reference sample with

repeatable reflectivity distribution, it was decided to compute surface shape using optical Monte-Carlo (MC) simulations and angular distribution data that were measured in our experiments.

3.1. Determining microstructure

Previous experience at Aalto University in characterization of gonioreflectometric properties of rough flat metal surfaces set a basis for our research. Studies carried out by Priit Jaanson *et al* [4] showed that for unpolarised light, a Torrance–Sparrow reflectance model [5] describes well the reflectance of plain aluminium surfaces. This model is based on geometrical optics and describes surface roughness as a number of microfacets that are oriented according to a specified distribution. For the latter, Gaussian [6] or Beckmann [7] distributions are often used. They parametrize surface roughness and, hence, allow to determine surface microstructure through a number of constants. In case of the Gaussian distribution, it is possible using a single parameter—root mean square slope σ of surface microfacets.

Fitting the reflection distribution function of the Torrance–Sparrow surface simulated by MC to the measured angular distribution of the reflectance sample under consideration allows one to estimate its roughness by obtaining the value of σ. In this case, the probability ρ that a ray coming from direction θ_i is reflected in the direction θ_v is

$$\rho(\theta_v) = \frac{1}{\pi}\left(D\cos(\theta_v) + S\,\frac{F(n,k)\,T(\sigma)\,A}{4\cos(\theta_i)\cos(\theta_v)}\right)d\theta_v \qquad (1)$$

where function $F(n,k)$ is given by Fresnel equations, $T(\sigma)$ is the Gaussian distribution of sample microfacets' slopes, σ is root mean square slope, A is associated geometric attenuation term and D and S are the ratios of diffusely and specularly reflected radiation, respectively. Parameters n,k are the index of refraction and extinction coefficient corresponding to the surface material and specified illumination wavelength. These parameters are chosen for the specified material and are held constant during fitting. Parameters D, S and σ are varied and the square sum of residuals between simulated and measured angular distributions are minimized to ensure the best fit.

To estimate the roughness of aluminium reflective insulator surface, we used $n = 9.1528$ and $k = 47.199$ obtained from [6] at the wavelength of $\lambda = 5$ μm and run MC simulation with the parameters close to the actual measurement, i.e. incidence angle $\theta_i = 11.5°$ and illumination spot size $d = 12$ mm. The result is depicted in figure 3 where the fitted parameters are $D = 0.0807$, $S = 2.2528$ and $\sigma = 0.0101$. Goodness of the fit was estimated by R-squared coefficient of determination:

$$R^2 = 1 - \frac{\sum_t \left(x_{f_t} - x_{m_t}\right)^2}{\sum_t \left(x_{m_t} - \overline{x_m}\right)^2} \qquad (2)$$

where x_{f_t} is the fitted value, x_{m_t} is the measured value and $\overline{x_m}$ is the average of measured values.

As expected, fitted parameters indicate that the flattened aluminium foil behaves mostly as a specular reflector since it has quite large specular ratio S and small diffuse reflectance ratio D. At the same time the root mean square slope of microfacets was greater than zero $\sigma > 0$ indicating that the aluminium foil surface is slightly rough.

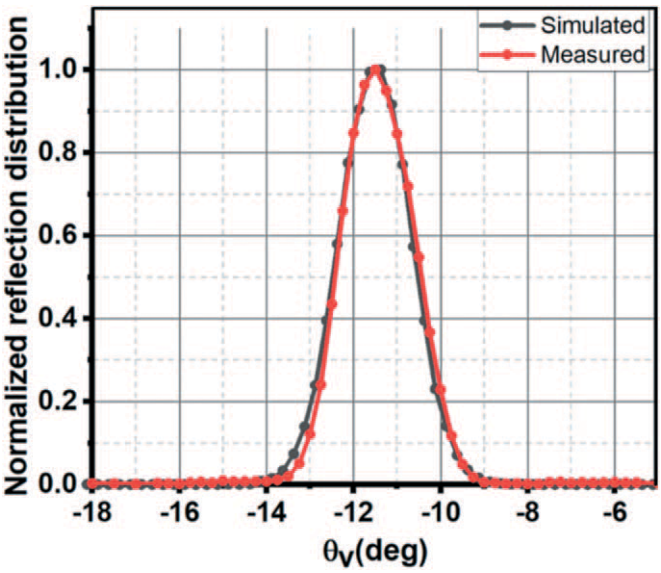

Figure 3. Result of the fitting of flat insulation foil's reflection distribution simulated by Monte Carlo (black curve) to the one measured by a gonioreflectometer (red curve). $R^2 = 0.995$.

According to Le and Sutcliffe, typical dimensions of microstructure waves on a cold-rolled aluminium foil surface are 25–50 μm for the wavelength and 0.25–0.50 μm for the amplitude [8]. The slope range calculated from these parameters is 0.005–0.01. The value of $\sigma = 0.0101 \approx 0.01$ corresponds to the upper border of the range indicating that the mean profile amplitude of the sample is around $R_a = 0.25$ μm and mean profile wavelength is $R_\lambda = 25$ μm. Typical minimal layer thickness for modern additive manufacturing of metals (i.e. laser sintering) is 20–50 μm [9]. Therefore, R_a is too small to be meaningful to pursuit with additive manufacturing production. Sandblasting with the fine sand and polishing the surface of a future reflectance reference sample seem to be, in this case, more reasonable methods for creating the desired surface microstructure.

3.2. Determining macrostructure

3.2.1. Distribution of macrofacets' normals. Modelling a foil surface shape is a complex task. Theoretically, for a given distribution of macrofacets' normals, the foil can be bended, folded and crumpled in an infinite amount of ways. As a result, a clear model for describing foil-like surfaces is absent. Most of the authors that tried to consider this problem rely on random surface models, such as random midpoint displacement method [10, 11] or spectral synthesis techniques [12, 13]. Both methods can be successfully used to produce naturally looking crumpled surfaces. However, they lack control over the distribution of macrofacets' normals and do not allow to model a random surface with a defined distribution.

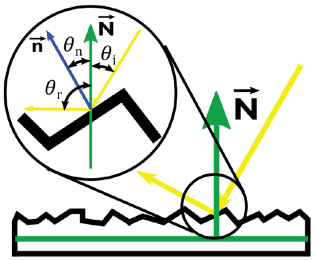

Figure 4. An example of a surface that is divided to a number of macrosurfaces with definitions of related geometrical quantities.

Fortunately, as confirmed with our measurements and simulations, the aluminium foil exhibits mostly specular reflection. This allows to derive the distribution of macrofacets' normals using measured angular reflection distribution and geometrical optics approach as it was done in the Torrance–Sparrow model. The aluminium surface can be divided to a number of mirror-like macrofacets, whose normal $\vec{n}$ orientation or slope corresponds to angle θ_n between macrofacet's normal $\vec{n}$ and the normal of the whole sample $\vec{N}$ as shown in figure 4.

Angle θ_n can be calculated knowing the angle of incidence θ_i and reflection angle θ_r:

$$\theta_n = \frac{\theta_i + \theta_r}{2} - \theta_i = \frac{\theta_r - \theta_i}{2} \tag{3}$$

This approach allows to convert the measured angular reflection distribution to the distribution of sample macrofacets' normals. In this case the reflection angles θ_r are converted to macrofacet normal angles θ_n using (3) and reflection values $r\left(\theta_{r_k}\right)$ are divided by the sum of all reflection values $\sum_k r\left(\theta_{r_k}\right)\cos\left(\theta_n + \theta_i\right)$ so that new values $\rho\left(\theta_n\right)$ would show which fraction of the whole surface area is aligned towards the direction corresponding to θ_n:

$$\rho\left(\theta_{n_k}\right) = \frac{r\left(\theta_{r_k}\right)}{\sum_v r\left(\theta_{r_v}\right)\cos\left(\theta_n + \theta_i\right)}. \tag{4}$$

θ_i is constant and $\cos\left(\theta_n + \theta_i\right)$ is required to take into account differences between viewed area and area of the facet directed towards $\vec{n}$.

One should note that $\rho\left(\theta_{n_k}\right)$ is not a continuous function and should be treated as a histogram since it represents the fraction of the surface corresponding to the surface normal angles' range $\theta_{n_k} = \pm\Delta\theta_n$ where $\Delta\theta_n = \left|\theta_{n_k} - \theta_{n_{k+1}}\right|$ in case of uniform angular steps. For this reason, if one would like to increase resolution of $\rho\left(\theta_{n_k}\right)$ by any kind of approximation, one should normalize $\rho\left(\theta_{n_k}\right)$ by the sum of its elements $\rho\left(\theta_{n_k}\right) = \rho\left(\theta_{n_k}\right) / \sum_v \rho\left(\theta_{n_v}\right)$ since the sum of all fractions should always be equal to 1.

In our case, angular reflection distribution of mesh reinforced foil was used to calculate macrofacets' normals' distribution of possible reflectance reference samples. Effects of measured sample non-uniformity were taken into account by averaging angular reflection distributions measured at different illumination spot positions. Obtained $\rho\left(\theta_{n_k}\right)$ was interpolated by a cubic spline and normalized to increase angular resolution. The result can be seen in figure 5.

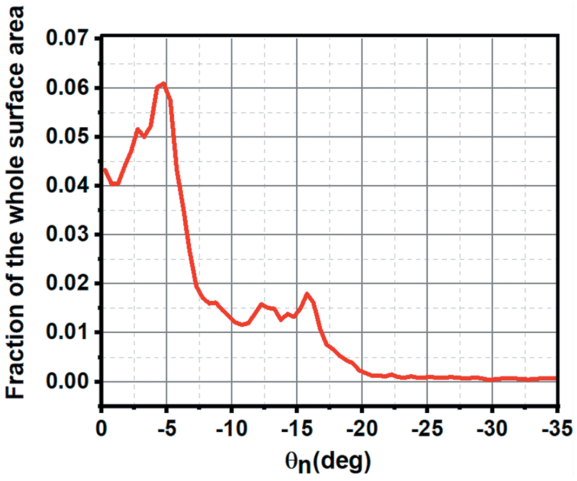

Figure 5. Distribution function of the normals of the microfacets $\rho\left(\theta_{nk}\right)$ calculated using (4) and the averaged data depicted in figure 2.

3.2.2. Facets' coalignment constrains. Macrofacets' normals distribution function $\rho\left(\theta_{n_k}\right)$ does not contain the full information about the surface. It describes only orientation of many individual surface facets, but provides no information about their coalignment. It can not, however, be completely random since we aim to develop surface with reflection distribution close to the actual sample and that requires a few constraints.

First, it is known that reflection was measured in one plane with the illumination that had a spot diameter of d and angle of incidence θ_i. In this case, the average illuminated distance projected to measurement plane will be the average of chords $\overline{a_b}$ that for a beam with radius r is

$$\overline{a_b} = \frac{\int_{0°}^{180°} 2r\sin\left(\frac{\alpha}{2}\right)d\alpha}{\cos\left(\theta_i\right)} = \frac{4r}{\pi}\frac{1}{\cos\left(\theta_i\right)} \tag{5}$$

where α is an angle between two radii forming triangle with the chord. For $d = 12$ mm it is around $\overline{a_b} = 7.71$ mm. Figure 2 indicates that the sample is reflecting illumination light to both sides around illumination direction. Assuming that there is an equal number of facets with normals pointing to the left and to the right of global normal $\vec{N}$ (figure 4), $d_c = \overline{a_b}/2 = 3.86$ mm is the characteristic distance of the surface within which there should be present enough elements to comprehensively manifest the distribution of normals $\rho\left(\theta_{nk}\right)$.

Second constraint emerges from the fact that distance $d_c = 3.86$ mm is too small for random coalignment of elements. For example, if we divide it to $K = 100$ elements then the length of a single element will be $l_e = 0.0386\ \text{mm} = 38.6\ \mu\text{m}$. The largest probable angle of surface normal, according to $\rho\left(\theta_{n_k}\right)$, is $\theta_{n_{max}} = 20°$ (figure 5). In this case the elevation of one of the facet's edges will be equal to $h_e = l_e\tan\left(\theta_{n_{max}}\right) = 14.05\ \mu\text{m}$. This is smaller than typical minimal layer thickness

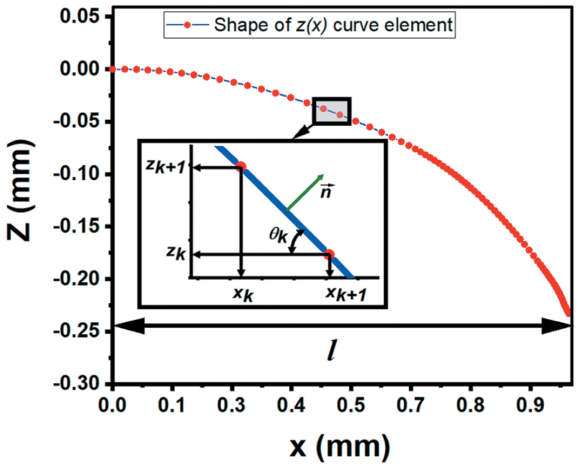

Figure 6. Part of surface profile $z(x)$ calculated using (6), (7), $K = 100$ and $l = 1$ mm.

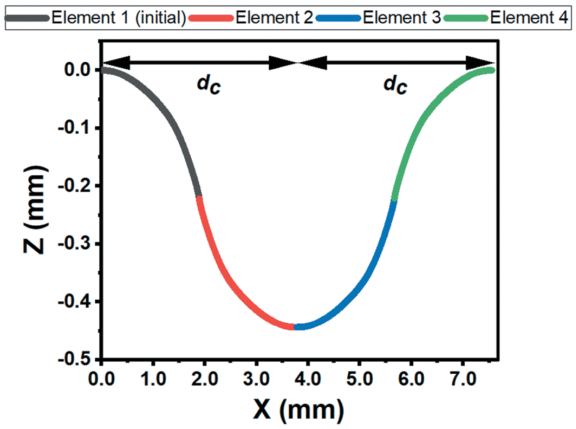

Figure 7. Single period of a waveform obtained from flipped and shifted elements $z_k = z(x_k)$.

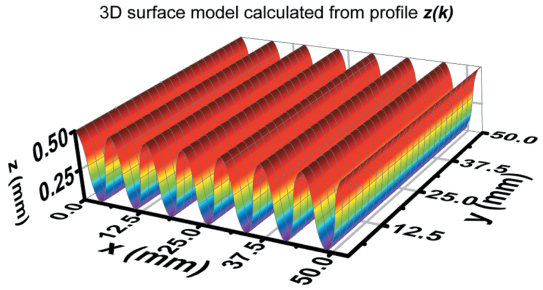

Figure 8. 3D model of structured reflectance reference sample for an aluminium foil.

(20–50 μm) of modern metal additive manufacturing facilities. If many of similar elements will be randomly coaligned, it may lead to features that are impossible to produce. Therefore, elements should be coaligned in a way where they would form larger structures with larger dimensions or they should be treated as microfacets instead.

Finally, to reduce the self-shadowing effect, obtuse angles between normals of two adjacent elements should be avoided. Otherwise it can cause unexpected changes in reflection distribution even though the surface normals are distributed according to $\rho(\theta_{n_k})$.

3.2.3. Surface shape. One of the solutions that satisfies imposed constraints is a waveform that is calculated by the following procedure.

Let us consider a surface whose profile in Cartesian coordinates is changing along X-axis and is constant along Y-axis. In this case, the surface profile can be completely described by the curve $z(x)$ projected onto X–Z plane. $z(x)$ can be divided to a number of parts with the length l along X-axis that itself is divided to K elements. Division of l is not uniform and is governed by normals' distribution $\rho(\theta_{n_k})$—the distance between two adjacent coordinates x_k and x_{k+1} $(k = 0 \ldots K)$ is proportional to the length of the segment with the normal angle θ_{n_k}, i.e. it represents the projection of fraction of the area $\rho(\theta_{n_k})$ onto X-axis and can be calculated as

$$|x_{k+1} - x_k| = l\rho(\theta_{n_k}) \cos(\theta_{n_k}) \tag{6}$$

where l has a role of scaling factor. Starting coordinate $x_{k=0}$ can be any and it defines the shift of the whole structure along X-axis. We set $x_{k=0}$ to 0. Values of curve $z_k = z(x_k)$ are calculated so that they would satisfy

$$|z_{k+1} - z_k| = |x_{k+1} - x_k| \tan(\theta_{n_k}) \tag{7}$$

and $z_{k=0}$ is also set to 0. The shape of a single part $z(x_k)$ for $K = 100$ and arbitrary $l = 1$ mm is depicted in figure 6.

Note that the step between angles θ_{n_k} and $\theta_{n_{k+1}}$ is constant and is equal to $\Delta\theta_n = |\theta_{n_0} - \theta_{n_{101}}| / K$, where $\theta_{n_0} = 0$ and $\theta_{n_{101}}$ are chosen according to values of $\rho(\theta_{n_k})$. In our case it was $\theta_{n_{101}} = -25°$. Moreover, since the angle between two adjacent normals is equal to $\Delta\theta_n$, there are no sharp angles between the facets.

The same principle should be used when connecting parts $z(x_k)$ to form a complete profile $z(x)$. This can be done by flipping and shifting parts $z_k = z(x_k)$ shown in figure 6. until they form a continuous waveform as shown in figure 7.

Note that the distribution of normals $\rho(\theta_{n_k})$ is comprehensively manifested already within l, but half of the surface directed to the right or to the left of global normal $\vec{N}$ is manifested only within $2l$. Therefore, the right selection for l would be $l = d_c/2$ that in case of $d_c = 3.86$ mm is 1.93 mm. In theory, the described selection should ensure that the reflection distribution will not vary with change of the position of a uniform illumination spot since there always will be a full period of $z(x)$ within distance $2d_c = \overline{a_c}$ (5). By this, all features of characteristic distance constraints are fulfilled.

Multiple periods of waveform can be stacked together to form a full profile curve $z(x)$ until it will describe a surface with reasonable dimensions. For example, 50 mm along X-axis. A 3D model can be then constructed from the obtained profile by stretching the profile along Y-axis. The result can be seen in figure 8.

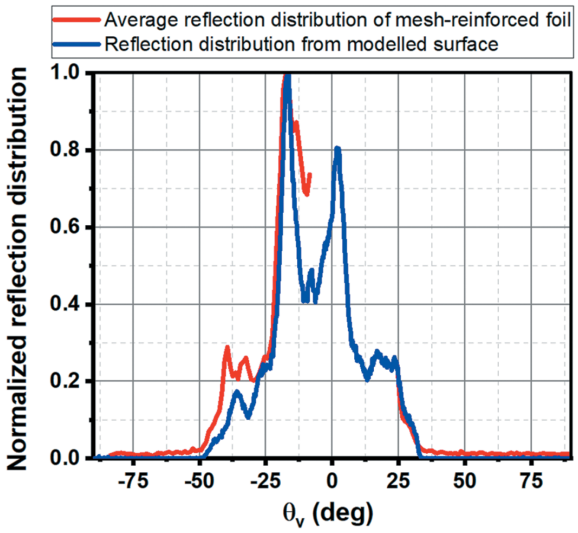

Figure 9. Reflection distribution function obtained using Monte-Carlo simulation on top of the distribution measured from the mesh-reinforced foil. Discontinuity of measured distribution is caused by instrumental limitations.

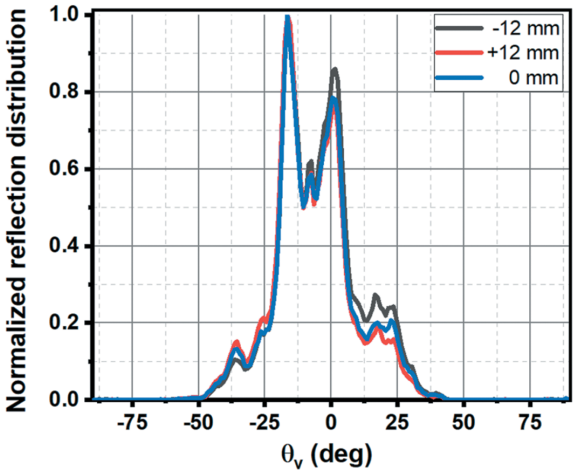

Figure 10. Reflection distribution functions of the virtual modelled surface for different positions of the illumination spot; obtained using Monte-Carlo simulations.

The dimensions of the obtained structure can be considered as macro since the height change along Z-axis is around 500 μm. It is larger than minimal layer thickness of 20 μm and may be produced by modern additive manufacturing of metals (i.e. laser sintering). However, some accuracy losses are inevitable and the produced sample might require a finishing sanding or polishing to eliminate possible step-like features.

4. Monte-Carlo experiments on generated surface

To validate the reflection distribution of the modelled reference reflectance sample surface, a Monte-Carlo ray-tracing simulation was performed. Simulation parameters were kept close to the ones used for mesh-reinforced foil measurements, i.e. the centre of virtual sample was illuminated by the beam with diameter of $d = 12$ mm and illumination angle of $\theta_i = 8°$. Illumination wavelength was kept at $\lambda_i = 5$ μm since the used software allowed to specify only one pair of index of refraction and extinction coefficient n and k. Values of $n = 9.1528$ and $k = 47.199$ were used. Reflection was modelled by Torrance–Sparrow model with parameters $D = 0.0807$, $S = 2.2528$ and $\sigma = 0.0101$ obtained from model fitting to reflection distribution of flat foil (see section 3.1). Altogether 180 virtual photosensors were placed around the sample in the plane of illumination to ensure angular resolution of 1° used during measurements. Corresponding collection solid angle of $\Omega \approx 0.001$ was also close to the collection solid angle of the instrument used for mesh-reinforced foil measurements. Paths of 10^7 photons were traced and the reflection distribution function for the presented 3D surface model was obtained. The result can be seen in figure 9.

The reflection distribution of the modelled surface is fairly close to the original average reflection distribution of the mesh-reinforced foil. The reflection maximum and the dispersion almost coincide and the overall shape is very similar. Complete identity of reflection distribution functions is not, however, the main goal. Presented similarity is sufficient for the planned reflectance reference sample. However, to fully fulfil this role, the modelled surface should also produce the same reflection distribution in case of different illumination spot positions. To validate whether the presented model exhibits this property, another set of MC simulations was run. Parameters remained the same. Only the position of illumination spot on the modelled surface was changed. first to -12 mm and then to $+12$ mm along X-axis. The result is presented in figure 10.

As can be seen, reflection distribution functions simulated for different illumination spot positions are fairly close to each other. Positions of main maxima and dispersion remain the same and only amplitudes of some of the maxima change. Quantitatively this change can be expressed in terms of the standard deviation of mean area under M reflection distributions $R_i(\theta_v)$:

$$\sigma_A = \sqrt{\frac{\sum_{i=1}^{M}\left(\int_{-90}^{90} R_i(\theta_v)\,d\theta_v - \overline{\int_{-90}^{90} R(\theta_v)\,d\theta_v}\right)^2}{M-1}}. \quad (8)$$

Ultimately, σ_A represents the standard uncertainty of total hemispherical reflectivity associated with the sample's non-uniform shape and/or change of measurement conditions. For simulated results it was $\sigma_A = 1.11$ that corresponds to 4.4 % deviation of area under reflection distribution and hence total hemispherical reflectivity.

5. Discussion

Deviation of total hemispherical reflectivity measured by working group CEN/TC 89/WG 12 is 6 %. Therefore, standard deviation of 4.4 %, coming from the modelled surface, is not sufficient to significantly improve the uncertainty of reflectivity measurements. This indicates that in practice, the length

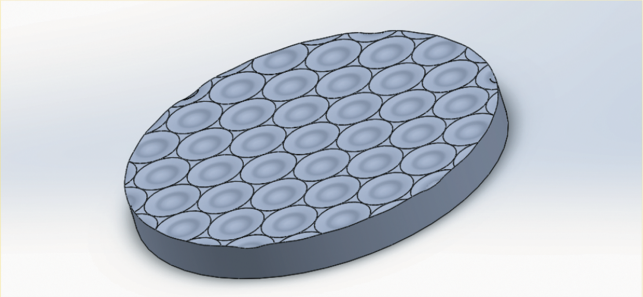

Figure 11. 3D model of structured reflectance reference sample formed from bell-shaped circular elements aligned in close-packing configuration.

$l = d_c/2$ of a single part $z_k = z(x_k)$ is not short enough to fully eliminate spatial variation of the reflection distribution function. MC simulations showed that reducing it to $l = d_c/4$ significantly improves the result—standard deviation σ_A becomes equal to 0.17 that makes 0.65 % of mean area under reflection distribution. Therefore, using this kind of sample as a reference might improve uncertainty of total hemispherical reflectivity measurements by up to a factor of 10. Further reduction of l might improve the result even more.

The only drawback of reduction of distance l is that the amplitude of surface waveform also diminishes and comes closer to the limits of additive manufacturing capabilities, increasing the uncertainty of surface production. A better approach might be to increase the illumination spot size. Additional MC simulations showed that increasing illumination spot size twice results in 0.65 % deviation of integral reflection distribution. That is exactly the same effect as decreasing the length l down to $d_c/4$.

Another issue that can affect the uncertainty of total hemispherical reflectivity measurements, is the anisotropy of modelled reflectance reference target's surface shape. In practice, it may be difficult to align a target that exhibits its properties only in one particular direction and misalignment can cause additional deviations in measurement results. Therefore, isotropic target is preferable.

One way to model such a target is to take one period of a waveform $z(x)$ presented in figure 7 and rotate it around Z-axis. It will produce a bell-shaped 3D element whose surface follows normals' distribution $\rho\left(\theta_{n_k}\right)$. Single elements can be then stacked together in hexagonal close packing configuration that is required to minimize flat space between elements figure 11. If too much space is left between elements, it will cause a significant change in the shape of reflection distribution that may be unacceptable for a reference sample. This problem, however, can be completely avoided by using spectral analysis.

By theory, in spatial frequency domain, isotropic surfaces have radially symmetrical 2D power spectra [14]. Therefore, if we apply Fourier transformation to the surface profile $z(x)$ and rotate its 1D power spectrum, we may generate the 2D spectrum of isotropic surface. Inverse Fourier transform of this 2D spectrum should produce a shape that follows normals' distribution $\rho\left(\theta_{n_k}\right)$ in all directions.

Application of the suggested methods and validation of reflection distribution of isotropic surface models is the scope of our future research.

6. Conclusion

The presented method for determination of macrofacets' distribution, combined with suggested constraints, can be successfully used to produce a fairly good surface model for the reflectance reference sample that would more accurately represent reflective insulators. Model dimensions indicate that, with some accuracy losses and proper finishing, it is feasible to produce such a sample with additive manufacturing. However, some additional work is required to model the isotropic surface shape.

Acknowledgements

This work was funded through the European Metrology Programme for Innovation and Research (EMPIR) Project 16NRM06 'EMIRIM'. The EMPIR initiative is co-funded by the European Union's Horizon 2020 research and innovation programme and the EMPIR Participating States.

ORCID iD

Dmitri Lanevski https://orcid.org/0000-0002-2465-6173

References

[1] Expression by the standardisation group CEN/TC 89/WG 12: the need for improvement of total hemispherical emissivity of low emissivity foils used in reflective insulation products 2017 https://www.giordano.it/uploaded-files/primopiano/16NRM06_Publishable_Summary.pdf (Accessed: 19 June 2019)

[2] Kononogova E, Adibekyan A, Monte C and Hollandt J 2019 Characterization, calibration and validation of an industrial emissometer *J. Sens. Sens. Syst.* **8** 233–42

[3] Scoarnec V, Hameury J, Verdure A, Blanchin A, Raulet D and Hay B 2014 Development of an absolute reflectometer for reflectance calibration of mirrors in the infrared *Rev. Fr. Métrol.* **2014** 29–38

[4] Jaanson P, Manoocheri F, Mäntynen H, Gergely M, Widlowski J-L and Ikonen E 2014 Gonioreflectometric properties of metal surfaces *Metrologia* **51** S314

[5] Sparrow E M, Torrance K E and Birkebak R C 1967 Theory for off-specular reflection from roughened surfaces *J. Opt. Soc. Am.* **57** 1105–14

[6] Cook R and Torrance K 1982 A reflectance model for computer graphics *ACM Trans. Graph.* **1** 7–24

[7] Rakić A D 1995 Algorithm for the determination of intrinsic optical constants of metal films: application to aluminum *Appl. Opt.* **34** 4755–67

[8] Le H R and Sutcliffe M P F 2000 Analysis of surface roughness of cold-rolled aluminium foil *WEAR* **244** 71–78

[9] Vaezi M, Seitz H and Yang S 2012 A review on 3D micro-additive manufacturing technologies *Int. J. Adv. Manuf. Technol.* **67** 1721–54

[10] Fournier A, Fussel D and Carpenter L 1982 Computer rendering of stochastic models *Commun. ACM* **25** 371–84

[11] Gavin M S P 1986 The definition and rendering of terrain maps *ACM SIGGRAPH Comput. Graph.* **20** 39–48
[12] Gelbaum Z and Titus M 2013 Simulation of fractional Brownian surfaces via spectral synthesis on manifolds *IEEE Trans. Image Process.* **23** 4383–8
[13] Bourke P 1997 Frequency synthesis of landscapes (and clouds) (http://paulbourke.net/fractals/noise/) (Accessed: 17 February 2020)
[14] Jacobs T D B, Jungle T and Pastewka L 2017 Quantitative characterization of surface topography using spectral analysis *Surf. Topogr. Metrol. Prop.* **5** 013001